Deadbeat Direct Flux Vector Control of Surface Permanent Magnet Motor Drives

Deadbeat Direct Flux Vector Control of Surface Permanent Magnet Motor Drives

S. Rubino, R. Bojoi, E. Armando, A. Tenconi
Dipartimento Energia "G. Ferraris"
Politecnico di Torino
Torino, 10129, Italy

***Abstract*—The predictive control algorithms for electrical drives are currently subject to considerable interest and development. In particular, the predictive torque control is a competitive solution that may replace in the future the conventional control schemes based on linear controllers. Therefore, the paper proposes a predictive torque control for surface permanent magnet motor drives requiring a wide constant power range. The predictive algorithm uses a deadbeat direct flux vector control approach for the simultaneous control of the stator flux amplitude and torque-producing current component. The proposed control scheme is suitable for applications requiring a wide speed range with current and voltage constraints. The proposed deadbeat torque controller has been tested on a fractional slot permanent magnet machine and the experimental results demonstrate the full drive controllability, including deep flux-weakening operation with limitation of the load-angle.**

Keywords—model predictive control, deadbeat control, direct flux vector control, permanent magnet motor drive.

NOMENCLATURE

(x, y)	Generic rotating frame.
(d, q)	Rotor frame.
(α, β)	Stationary frame.
(d_s, q_s)	Stator flux linkage frame.
$_{dqs}$	Subscript – (d_s, q_s) abbreviation.
$\overline{z}_{xy} = \begin{bmatrix} z_x & z_y \end{bmatrix}^t$	Generic vector defined in the generic (x, y) frame.
$\overline{v}_{s,xy} = \begin{bmatrix} v_{s,x} & v_{s,y} \end{bmatrix}^t$	Stator voltage vector defined in the generic (x, y) frame.
$\overline{i}_{s,xy} = \begin{bmatrix} i_{s,x} & i_{s,y} \end{bmatrix}^t$	Stator current vector defined in the generic (x, y) frame.
$\overline{\lambda}_{s,xy} = \begin{bmatrix} \lambda_{s,x} & \lambda_{s,y} \end{bmatrix}^t$	Stator flux linkage vector defined in the generic (x, y) frame.
$\overline{\lambda}_{m,xy} = \begin{bmatrix} \lambda_{m,x} & \lambda_{m,y} \end{bmatrix}^t$	PM flux linkage vector defined in the generic (x, y) frame.
$\overline{u}_{s,xy} = \begin{bmatrix} u_{s,x} & u_{s,y} \end{bmatrix}^t$	Input voltage vector defined in the generic (x, y) frame.
$\overline{e}_{s,xy} = \begin{bmatrix} e_{s,x} & e_{s,y} \end{bmatrix}^t$	Back-emf voltage vector defined in the generic (x, y) frame.
$\overline{v}_{s-rec,xy} = \begin{bmatrix} v_{s-rec,x} \\ v_{s-rec,y} \end{bmatrix}$	Reconstructed stator voltage vector defined in the generic (x, y) frame.
$\overline{v}_{dt,xy} = \begin{bmatrix} v_{dt,x} & v_{dt,y} \end{bmatrix}^t$	DT voltage error vector defined in the generic (x, y) frame.
$j = \begin{bmatrix} 0 & -1 \\ 1 & 0 \end{bmatrix}$	Complex vector operator.
ϑ_m	Mechanical rotor position.
ϑ_r	Electric rotor position.
ϑ_s	Positon of stator flux linkage vector.
ω_{xy}	Synchronous speed of the generic (x, y) frame.
ω_m	Mechanical rotor speed.
ω_r	Electric rotor speed.
ω_s	Stator flux linkage vector speed.
p	Machine pole pairs.
R_s	Stator resistance.
L_s	Stator inductance.
λ_m	PM flux linkage.
λ_s	Stator flux linkage amplitude.
T	Electromagnetic torque.
δ	Machine load-angle. Anticlockwise angular deviation with respect to the physical d-axis.
ω_δ	Time derivative of the load angle.
$\boldsymbol{A}$, $\boldsymbol{b}$	State-space matrices in the continuous time-domain.
$\boldsymbol{A_d}$, $\boldsymbol{b_d}$	State-space matrices in the discrete time-domain.
a_{xx}, a_{xy}, b_{xx}, b_{xy}	$\boldsymbol{A_d}$, $\boldsymbol{b_d}$ matrices' coefficients.
T_s	Sampling period.
f_s, k_s, φ_s	Preliminary variables.
τ	Sample time instant.
*	Superscript – reference value.
$\tilde{}$ / $\hat{}$	Superscripts – estimated value.
$\hat{}$	Superscript – observed value.
ω_c	Observer gain.
q	Laplace domain variable.
z	Discrete domain variable.
$v_{s,abc}$	Stator voltage vector in phase coordinates.
$i_{s,abc}$	Stator current vector in phase coordinates.
$v_{dt,abc}$	DT voltage error vector in phase coordinates.
d^*_{abc}	Inverter duty cycles commands.
v_{dc}	DC – link voltage.
I_{max}	Phase currents amplitude limit.
δ_{max}	Load-angle limit.
$v_{s,max}$	Phase voltages limit.
$\lambda^*_{s,\mathrm{MTPA}}$	MTPA stator flux reference.
$\lambda_{s,max}$	Upper limit of stator flux amplitude.
$\lambda_{s,min}$	Lower limit of stator flux amplitude.
$i^\tau_{s,qs-maxi}$	q_s – axis current saturation limit due to $I_{max.}$
$i^\tau_{s,qs-max\,\delta}$	q_s – axis current saturation limit due to $\delta_{max.}$
$v_{sd,max}$	d_s – axis reference voltage limit.

I. Introduction

The Model Predictive Control (MPC) represents one of the most promising evolutions in the field of electric drives [1]. The use of MPC schemes allows at obtaining better dynamic performance and a less demanding tuning procedure with respect to the conventional control schemes based on linear controllers, as there are no controller gains to be calibrated during the final drive tests for the application.

The literature reports two main MPC solutions [1]: (1) Finite Control Set Model Predictive Control (FCS-MPC) and (2) Continuous Control Set Model Predictive Control (CCS-MPC). The main difference between these two solutions is related to the computation of the inverter voltage commands. In FCS-MPC schemes, the voltage commands are selected among the inverter discrete states, using a specific cost function [2], [3], and without the use of Pulse Width Modulation (PWM). Therefore, the inverter switching frequency is variable. Compared to the FCS-MPC algorithms, the outputs of a CCS-MPC scheme correspond to all possible average inverter voltage vectors, making necessary the use of a PWM modulator [4]. Consequently, the inverter switching frequency is constant and synchronized with the sampling frequency.

The choice of the MPC scheme depends on the application. For example, in high power/high current systems where the converter switching frequency is strictly limited at low values, the use of FCS-MPC is a compromise between good drive performance and low inverter switching frequency, with the expense of inherent high current distortion and high torque ripple [5].

For applications where the inverter switching frequency is high (>10 kHz), the CCS-MPC yields both high dynamic performance with very low current distortion and low torque ripple. The most popular version of the CCS-MPC is the Deadbeat Control (DB) that calculates the voltage commands to get the best dynamic drive performance. Indeed, for small variations of the reference, the output reaches the target in one beat (sampling time). For example, the literature reports the DB Torque and Flux Control (DB-FTC) [6]–[11], for simultaneous stator flux amplitude and torque control of both induction and permanent magnet machines. This solution is an evolution of the Direct Torque Control (DTC) to make it predictive, performed at a constant switching frequency. Furthermore, it inherits all the advantages of the DTC in terms of high dynamic performance.

However, except for high power, medium voltage drives, the application of the MPC schemes in the industry is somewhat limited. One reason can be the dynamic behavior of the MPC schemes working with voltage limitation. This condition is quite critical as it usually corresponds to the deep flux-weakening near the pull-out limit, corresponding to the Maximum-Torque per Volt (MTPV) operation. The technical literature contains very few solutions that deal with these operating conditions, except for the already mentioned DB-FTC [6]–[9]. The results achieved with the DB-FTC are proof of how the direct stator flux amplitude regulation is a key factor for the robustness and feasibility of an MPC scheme able to deal with the full speed range of a motor drive.

An alternative to the direct flux amplitude and torque regulations is the Direct Flux Vector Control (DFVC) recently proposed in [12], using linear controllers. The DFVC is implemented in the stator flux synchronous reference frame and performs a direct stator flux amplitude regulation. However, compared to the FTC approach, the DFVC performs an indirect torque regulation through the regulation of the torque-producing current component. In this way, the DFVC linearizes the torque expression, while the flux regulation and the torque-producing current are quite decoupled. In addition, the DFVC allows a straightforward current limitation, as for the Field Oriented Control (FOC) using inner current control loops with linear controllers. Therefore, the DFVC can easily guarantee the maximum torque production under both current and voltage limitations, including MTPV operation.

This paper proposes a DB-DFVC for Surface Permanent Magnet (SPM) motors employed in applications that require deep flux weakening operation with a wide constant power range, including MTPV operation. The proposed solution has the following features:

- Direct stator flux amplitude regulation (as for DB-FTC).
- Direct torque-producing current regulation allowing straightforward current limitation (as for FOC with inner current control loops).
- High-performance in the dynamic torque response (as for any DB scheme).
- Straightforward flux weakening operation, avoiding any outer flux loop or voltage limitation loop that limits the dynamic performance, as happens for the conventional FOC schemes. In addition, the torque regulation at flux weakening, including MTPV operation with direct load-angle limitation, does not require machine maps or Look-Up Tables.
- With proper knowledge of the machine parameters, no tuning is necessary for the torque control, as required for the conventional FOC schemes.
- With respect to the DB-FTC, the dynamics of the two control axes are quite independent of each other. Moreover, the DB-DFVC uses a simple current estimator instead of a current observer, resulting simpler when compared with DB-FTC.

The performance of the proposed DB-DFVC has been validated on a low-power, fractional slot SPM machine with concentrated windings. The machine design allows flux-weakening operation in a wide constant power range. This paper extends the results presented in [13], by including: small and large step torque transient responses, effects of detuning of machine parameters, and the verification of torque regulation bandwidth. A comparison with the DFVC using linear controllers has been also included.

The paper is organized as follows. The machine modeling with the introduction of the state-space equations and their discretization is described in Section II. The proposed deadbeat control scheme is shown in Section III, while the experimental results are provided in Section IV. Finally, Section V concludes the paper.

II. Discrete-time modeling of a SPM machine

The implementation of any model-based predictive algorithm requires a proper discrete model of the considered system. Therefore, it is necessary to define first the SPM machine state-space model in continuous time-domain. Then, it is mandatory to define an accurate discretization method to

convert the state-space equations from the continuous time-domain to the discrete one.

A. Machine modeling

The SPM machine electromagnetic model can be obtained using the unified theory of the electrical machines [14]. The stator electric model is computed as:

$$\bar{v}_{s,dq} = R_s \cdot \bar{i}_{s,dq} + \frac{d}{dt}\bar{\lambda}_{s,dq} + j \cdot \omega_r \cdot \bar{\lambda}_{s,dq} \tag{1}$$

where the *d*-axis is conventionally defined as the *N*-pole direction of the magnets.

According to the magnetic model (or current model), the stator flux is computed as:

$$\bar{\lambda}_{s,dq} = L_s \cdot \bar{i}_{s,dq} + \bar{\lambda}_{m,dq} = L_s \cdot \bar{i}_{s,dq} + \begin{bmatrix}\lambda_m & 0\end{bmatrix}^t \tag{2}$$

where the term λ_m represents the amplitude of stator flux linkage caused by the permanent magnets (PM) only. Finally, the electromagnetic torque T is:

$$T = \frac{3}{2} \cdot p \cdot \left(\bar{\lambda}_{s,dq} \wedge \bar{i}_{s,dq}\right) \tag{3}$$

By denoting with δ the anticlockwise angular deviation with respect to the physical *d*-axis, the electromagnetic model (1)-(3) can be referred to a generic (*x*, *y*) frame as:

$$\begin{cases} \bar{v}_{s,xy} = R_s \cdot \bar{i}_{s,xy} + \dfrac{d}{dt}\bar{\lambda}_{s,xy} + j \cdot \omega_{xy} \cdot \bar{\lambda}_{s,xy} \\ \bar{\lambda}_{s,xy} = L_s \cdot \bar{i}_{s,xy} + \bar{\lambda}_{m,xy} = L_s \cdot \bar{i}_{s,xy} + \lambda_m \cdot e^{-j\cdot\delta} \\ T = \dfrac{3}{2} \cdot p \cdot \left(\bar{\lambda}_{s,xy} \wedge \bar{i}_{s,xy}\right) \end{cases} \tag{4}$$

where ω_{xy} is the synchronous speed of the generic (*x*, *y*) frame and defined as:

$$\omega_{xy} = \omega_r + \frac{d\delta}{dt} = \omega_r + \omega_\delta \tag{5}$$

Starting from the electromagnetic model (4), the computation of the state-space equations in the canonical form leads to:

$$\frac{d}{dt}\begin{Bmatrix} i_{s,x} \\ i_{s,y} \end{Bmatrix} = \boldsymbol{A} \cdot \begin{Bmatrix} i_{s,x} \\ i_{s,y} \end{Bmatrix} + \boldsymbol{b} \cdot \begin{Bmatrix} u_{s,x} \\ u_{s,y} \end{Bmatrix} \tag{6}$$

where the parametric matrices $\boldsymbol{A}$ and $\boldsymbol{b}$ are computed as:

$$\boldsymbol{A} = \begin{bmatrix} -\dfrac{R_s}{L_s} & \omega_{xy} \\ -\omega_{xy} & -\dfrac{R_s}{L_s} \end{bmatrix} \qquad \boldsymbol{b} = \frac{1}{L_s} \cdot \begin{bmatrix} 1 & 0 \\ 0 & 1 \end{bmatrix} \tag{7}$$

while the input vector $\bar{u}_{s,xy}$ is given by:

$$\begin{Bmatrix} u_{s,x} \\ u_{s,y} \end{Bmatrix} = \begin{Bmatrix} v_{sx} + \omega_r \cdot \lambda_{m,y} \\ v_{sy} - \omega_r \cdot \lambda_{m,x} \end{Bmatrix} = \begin{Bmatrix} v_{sx} - \omega_r \cdot \lambda_m \cdot \sin(\delta) \\ v_{sy} - \omega_r \cdot \lambda_m \cdot \cos(\delta) \end{Bmatrix} \tag{8}$$

The equations (6)-(8) have a high degree of versatility as they can be referred to any reference frame by changing the meaning of the variable δ, as shown in (9).

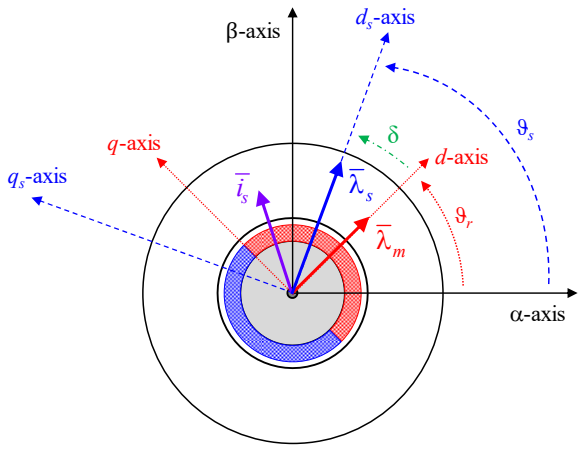

Fig. 1. Stationary (α,β) frame, stator flux (d_s,q_s) frame, and rotor physical (*d*,*q*) frame for a 2-pole SPM machine.

$$\begin{aligned} &(a)\ \delta = 0, && \omega_{xy} = \omega_r, && (x,y) = (d,q)\ \text{rotor frame} \\ &(b)\ \delta = -\vartheta_r, && \omega_{xy} = 0, && (x,y) = (\alpha,\beta)\ \text{stationary frame} \\ &(c)\ \delta = \vartheta_s - \vartheta_r, && \omega_{xy} = \omega_s, && (x,y) = (d_s,q_s)\ \text{stator flux frame} \end{aligned} \tag{9}$$

The (9)-c) is the stator flux frame where the DB-FTC and DVFC schemes are implemented. In this specific case, the variable δ has the meaning of the machine load-angle, as shown in Fig. 1. Given the electromagnetic torque, the load-angle depends on the amplitude of the stator flux.

B. Discrete time-domain conversion

Based on the technical literature, several methods can be employed to convert the state-space equations from the continuous time-domain to the discrete one. Due to its simplicity, the Euler method is usually employed. However, to minimize the discretization error when the ratio between the sampling frequency and fundamental frequency becomes too low, an accurate method must be used. According to [15], the discretization of the (6) leads to the following structure:

$$\begin{Bmatrix} i_{s,x}(\tau+1) \\ i_{s,y}(\tau+1) \end{Bmatrix} = \boldsymbol{A_d} \cdot \begin{Bmatrix} i_{s,x}(\tau) \\ i_{s,y}(\tau) \end{Bmatrix} + \boldsymbol{b_d} \cdot \begin{Bmatrix} u_{s,x}(\tau) \\ u_{s,y}(\tau) \end{Bmatrix} \tag{10}$$

where τ represents the generic sample time instant. The discrete matrices $\boldsymbol{A_d}$ and $\boldsymbol{b_d}$ are computed as follows [15]:

$$\boldsymbol{A_d} = e^{\boldsymbol{A}\cdot T_s} \qquad \boldsymbol{b_d} = \int_0^{T_s} \left(e^{\boldsymbol{A}\cdot t} \cdot \boldsymbol{b}\right) dt \tag{11}$$

The sample period for the discretization T_s can be set arbitrary within the limits of the cardinal theorem of interpolation. In practice, it corresponds with the sampling time of the machine control. For the sake of clarity, the following preliminary variables are introduced:

$$f_s = R_s / L_s \quad , \quad k_s = e^{-f_s \cdot T_s} \quad , \quad \varphi_s = \omega_{xy} \cdot T_s \tag{12}$$

The application of (11) on (7) leads to the following structure of the discrete matrices:

$$\boldsymbol{A_d} = \begin{bmatrix} a_{xx} & a_{xy} \\ -a_{xy} & a_{xx} \end{bmatrix} \qquad \boldsymbol{b_d} = \begin{bmatrix} b_{xx} & b_{xy} \\ -b_{xy} & b_{xx} \end{bmatrix} \tag{13}$$

where the coefficients are computed as follows:

$$\begin{cases} a_{xx} = k_s \cdot \cos(\varphi_s) \\ a_{xy} = k_s \cdot \sin(\varphi_s) \end{cases} \tag{14}$$

$$\begin{cases} b_{xx} = \dfrac{1}{R_s} \cdot \dfrac{f_s}{f_s^2 + \omega_{xy}^2} \cdot \left[f_s \cdot (1 - a_{xx}) + \omega_{xy} \cdot a_{xy} \right] \\ b_{xy} = \dfrac{1}{R_s} \cdot \dfrac{f_s}{f_s^2 + \omega_{xy}^2} \cdot \left[\omega_{xy} \cdot (1 - a_{xx}) - f_s \cdot a_{xy} \right] \end{cases} \tag{15}$$

The equation system (10)-(15) represents the discrete-time electromagnetic model of an SPM machine in a generic (*x, y*) frame. According to (10), the computed and/or measured variables at the sample time instant τ allow the prediction of the state-variables for the next one (τ+1). Furthermore, due to (11), the performance of the proposed discretization method depends only on the accuracy of the machine parameters.

III. Machine Control Scheme

The application of a predictive algorithm consists of a better computation of the voltage references to improve the performance of an already existing drive scheme. For this reason, all conventional control structures can still be used (FOC, constant switching frequency DTC, etc…). The only difference consists of replacing the conventional Proportional-Integral (PI) regulators with a predictive mechanism that depends on the adopted MPC solution (FCS or CCS).

A. Stator flux amplitude and torque equations

According to the torque demand and the operating speed, the DFVC performs the control of the stator flux vector and stator current vector in the stator flux synchronous frame [12]. Therefore, by applying the condition (9)-c) on the machine model (4), the following control equations are obtained:

$$\begin{cases} v_{s,ds} = R_s \cdot i_{s,ds} + \dfrac{d}{dt}\lambda_s \\ v_{s,qs} = R_s \cdot i_{s,qs} + \omega_s \cdot \lambda_s \\ \bar{\lambda}_{s,dqs} = L_s \cdot \bar{i}_{s,dqs} + \bar{\lambda}_{m,dqs} \\ T = \dfrac{3}{2} \cdot p \cdot \lambda_s \cdot i_{s,qs} \end{cases} \tag{16}$$

Except for the magnetic equation that is formally identical to (4), it is noted the linearization of the torque equation. Indeed, the torque depends on the product between the stator flux amplitude λ_s with the q_s-axis current component $i_{s,qs}$ that assumes a torque-producing current function. For this reason, in the DFVC scheme, the q_s-axis current component is chosen as the main control variable (together with the stator flux amplitude regulation), thus replacing the conventional direct torque regulation (as for FTC).

To understand better the advantages of the indirect torque regulation through the direct control of the torque-producing current component $i_{s,qs}$, it is necessary to compute the state-equations related to these variables. Therefore, by applying the condition (9)-c) in (6), the results reported in (17) are obtained.

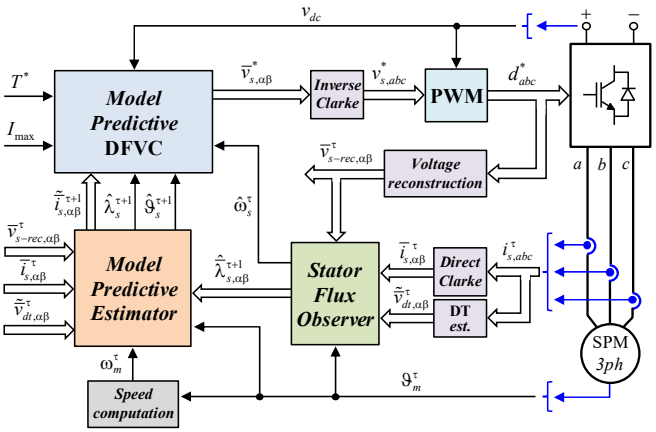

Fig. 2. Proposed predictive DFVC scheme for an SPM machine.

$$\begin{cases} \dfrac{d}{dt}\lambda_s = -\dfrac{R_s}{L_s} \cdot \lambda_s + v_{s,ds} + \dfrac{R_s}{L_s} \cdot \lambda_m \cdot \cos(\delta) \\ \dfrac{d}{dt} i_{s,qs} = -\omega_s \cdot i_{s,ds} - \dfrac{R_s}{L_s} \cdot i_{s,qs} + \dfrac{1}{L_s} \cdot \left(v_{s,qs} - \omega_r \cdot \lambda_m \cdot \cos(\delta) \right) \end{cases} \tag{17}$$

The model (17) leads to the following considerations:

- The stator flux amplitude λ_s can be directly regulated through the d_s-axis voltage component $v_{s,ds}$.
- The torque-producing current component $i_{s,qs}$ can be regulated through the q_s-axis voltage component $v_{s,qs}$.

But most of all, it is noted how the dynamics of the two control axes are quite independent of each other. The only coupling effects are related to the load-angle variation terms. However, they have the meaning of additive disturbance without any influence in the control dynamics. This aspect represents an impressive advantage with respect to the direct torque regulation whose state equation is given by a non-linear combination of the two above control dynamics, as in (18):

$$\frac{d}{dt} T = \frac{3}{2} \cdot p \cdot \left(i_{s,qs} \cdot \frac{d}{dt}\lambda_s + \lambda_s \cdot \frac{d}{dt} i_{s,qs} \right) \tag{18}$$

Therefore, through the DFVC scheme, it is possible to perform the vector control of an SPM machine using two independent scalar controls. Like a dc drive, the torque-producing current component can be considered as an equivalent armature current while the d_s-axis equation as an equivalent excitation mechanism.

The proposed scheme is shown in Fig. 2 and the descriptions of the different blocks are reported next.

B. Stator flux observer

The DFVC scheme is implemented in the rotating stator flux synchronous frame (d_s,q_s). Therefore, a stator flux observer must be implemented to obtain both amplitude and angular position of the stator flux vector. The flux observer is obtained as a linear combination of two model-based estimators performed in stationary reference frame (α,β), as shown in Fig. 3. In detail, the flux observer is based on the back-emf integration at high speed (voltage model - blue-window) and the current model (red-window) at low speed.

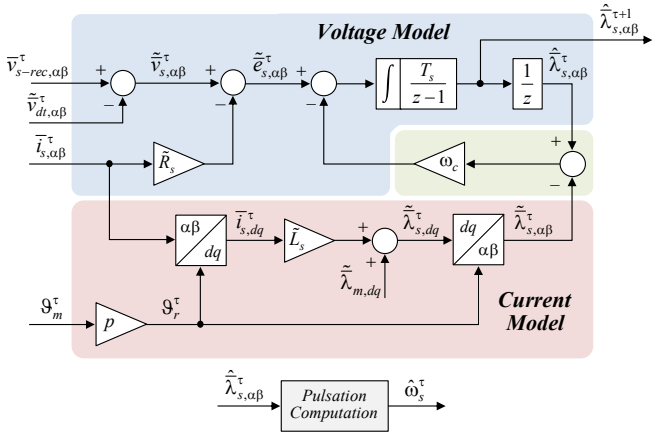

Fig. 3. Stator flux observer with predictive stator flux estimation.

The low-speed estimator is based on the magnetic model (2) defined in the physical (*d*,*q*) frame. Therefore, the stator currents measurements and the feedback on the *d*-axis position are necessary. The use of the magnetic model avoids the stator voltages reconstruction, making the flux estimation quite robust against the dead-time (DT) voltage errors. Furthermore, the absence of any time-integration guarantees the total immunity from any numeric drifting.

The high-speed estimator uses the back-emf integration to obtain the direct estimation of the stator flux components. The stator electric model is implemented in the stationary (α,β) frame. In this way, just the estimation of the back-emf voltages $\overline{e}_{s,\alpha\beta}$ is required. Therefore, the stator voltages reconstruction $\tilde{\overline{v}}_{s,\alpha\beta}$ is followed by the compensation of the voltage drops related to the stator resistance. The use of the stator electric model guarantees an accurate flux estimation especially in the medium/high-speed range of the drive. Indeed, in these operating conditions, the detuning on the stator resistance has shallow effects on the flux estimation, making the estimator quite robust and accurate. Besides, to improve the estimation of the back-emf voltages, a Dead-Time (DT) compensation scheme is proposed, using the solution described in [16].

Due to the execution delay of the digital control together with the inverter behavior, the use of the backward-Euler integration allows a straightforward prediction of the stator flux vector components, as shown in Fig. 3. In detail, starting from the back-emf voltage estimates at the current sample time instant τ, the prediction of the stator flux vector components for the next sample time instant (τ+1) is performed as:

$$\hat{\tilde{\overline{\lambda}}}^{\tau+1}_{s,\alpha\beta} = \hat{\tilde{\overline{\lambda}}}^{\tau}_{s,\alpha\beta} + T_s \cdot \tilde{\overline{e}}^{\tau}_{s,\alpha\beta} \tag{19}$$

The (19) is extremely accurate and robust. Furthermore, it avoids the implementation of an additional model predictive estimator for the prediction of stator flux vector components.

Finally, the transition electrical frequency (rad/s) between the two above reported estimators is set through the observer gain ω_c (Fig. 3), according to the following transition law:

$$\hat{\overline{\lambda}}_{s,\alpha\beta} = \tilde{\overline{\lambda}}_{s,\alpha\beta} \cdot \frac{\omega_c}{q+\omega_c} + \left(\frac{\tilde{\overline{e}}_{s,\alpha\beta}}{q}\right) \cdot \frac{q}{q+\omega_c} \tag{20}$$

where *q* represents the Laplace – domain variable.

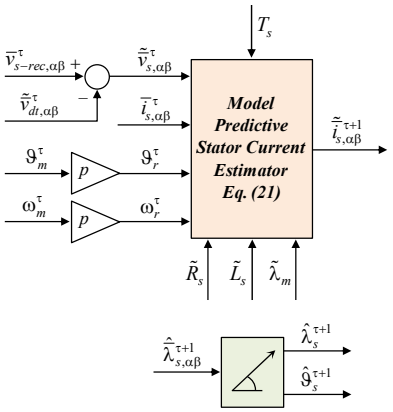

Fig. 4. Model predictive stator current estimator (MPE).

According to (20), the flux estimate obtained with the stator magnetic model corresponds with the observer output when the electrical speed is lower than ω_c. Conversely, the back-emf integration prevails when the electrical speed is higher than ω_c. The observer gain has been set at 125 rad/s, corresponding to 5% of the maximum electrical frequency (420 Hz) for the machine used in the experimental validation.

C. Model predictive estimator (MPE)

The stator flux observer performs the prediction of the stator flux vector components. However, the prediction of the stator current vector components is also needed. For this reason, a Model Predictive Estimator (MPE) must be implemented, as shown in Fig. 4.

According to (9), the stator current prediction can be performed in any reference frame. In this work, the stationary (α,β) frame is selected, leading to relevant simplifications of the discrete state-space equations. Indeed, the application of the condition (9)-b) on the discrete machine model (10) leads to as follows:

$$\tilde{\overline{i}}^{\tau+1}_{s,\alpha\beta} = \tilde{k}_s \cdot \tilde{\overline{i}}^{\tau}_{s,\alpha\beta} + \tilde{R}_s^{-1} \cdot \left(1-\tilde{k}_s\right) \cdot \left(\tilde{\overline{v}}^{\tau}_{s,\alpha\beta} - j \cdot \omega_r^{\tau} \cdot \tilde{\overline{\lambda}}^{\tau}_{m,\alpha\beta}\right) \tag{21}$$

The equation (21) allows the prediction of the stator current vector components for the next sample time instant (τ+1). It is noted how the stator current prediction results quite robust and simple to be performed.

D. Stator flux reference computation

The main inputs of the control scheme are the electromagnetic torque reference T^* and the phase currents amplitude limit I_{max} (usually related to the current limit of the power converter and/or the machine), as shown in Fig. 5. The reference torque is usually provided by an outer control loop that depends on the drive application. In this work, a speed controller will be considered.

Based on the torque reference, the optimal stator flux amplitude value is computed following the Maximum-Torque per Ampere (MTPA) torque-to-flux profile of the machine, as shown in Fig. 5. According to the machine model in the physical (*d*,*q*) frame (1)-(3), the MTPA operation corresponds to the injection of current on the *q*-axis. In terms of stator flux amplitude, this condition can be expressed as follows:

$$\lambda^*_{s,\mathrm{MTPA}} = \tilde{\lambda}_m \cdot \sqrt{1 + \frac{4}{9} \cdot \left(\frac{\tilde{L}_s \cdot T^*}{p \cdot \tilde{\lambda}_m^2}\right)^2} \tag{22}$$

This equation (22) is defined under the hypothesis of magnetic linearity. However, to improve efficiency, accurate machine mapping can be performed [17].

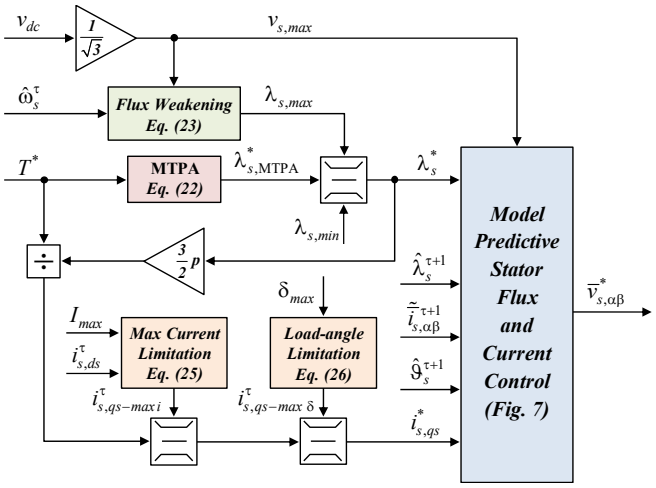

Fig. 5. Predictive DB-DFVC scheme: computation of the stator flux amplitude and torque-producing current references.

In this case, the optimal stator flux amplitude reference $\lambda^*_{s,\mathrm{MTPA}}$ is obtained using a pre-loaded look-up table (LUT). However, this corresponds with the flux reference λ^*_s only below the base speed.

Indeed, when the sinusoidal phase voltages limit of the inverter $v_{s,max}$ ($v_{dc}/\sqrt{3}$) is reached, the stator flux amplitude reference is limited to allow the drive operation under the voltage constraint. Based on (16), the stator flux amplitude limit is computed as:

$$\lambda_{s,max} \le \frac{\sqrt{v_{s,\max}^2 - \left(\tilde{R}_s \cdot i^{\tau}_{s,ds}\right)^2} - \tilde{R}_s \cdot i^{\tau}_{s,qs} \cdot sign\left(\hat{\omega}^{\tau}_s\right)}{\left|\hat{\omega}^{\tau}_s\right|} \quad (23)$$

where $\hat{\omega}^{\tau}_s$ is the synchronous speed of the stator flux vector at the current sample time instant τ, as shown in Fig. 3. However, to avoid any disturbance related to the load-angle variation (5), the synchronous speed is replaced with the rotor electrical one ω_r. It is noted how (23) leads to a straightforward Flux-Weakening (FW) regulation law (as for DTC and DB-FTC schemes), without the use of any voltage regulator (as for FOC schemes).

Finally, the stator flux amplitude reference is limited at the minimum value $\lambda_{s,min}$, as shown in Fig. 5. This limit is lower than the minimum value required at FW operation with the maximum motor speed and the minimum DC-link voltage.

E. Torque-producing current reference computation

Based on (16), the torque-producing current reference $i^*_{s,qs}$ is computed from the torque reference T^* and the reference of the stator flux amplitude λ^*_s as:

$$i^*_{s,qs} = \frac{T^*}{1.5 \cdot p \cdot \lambda^*_s} \quad (24)$$

The q_s-axis current reference (24) is subjected to two consecutive limitations, corresponding to the constraints of maximum current amplitude I_{max} and maximum load-angle δ_{max}, as shown in Fig. 5. The first saturation limit $i^{\tau}_{s,qs-maxi}$ does not depend on the torque sign but only on the current limit I_{max}, as reported in the equation (25).

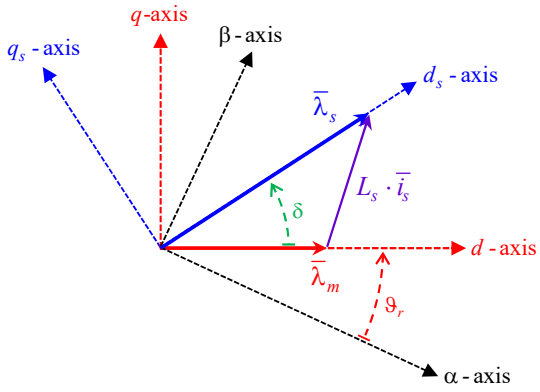

Fig. 6. Vector diagram representing the SPM machine magnetic model.

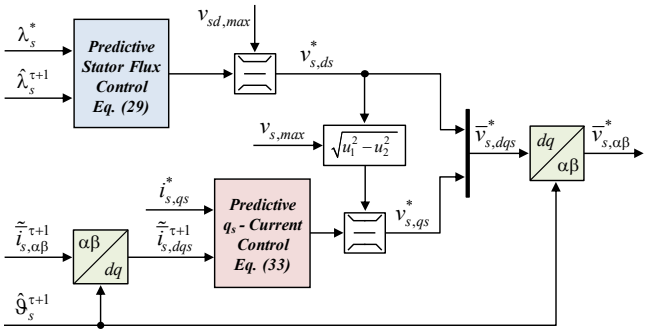

Fig. 7. Model predictive stator flux and current control.

$$\left|i^*_{s,qs}\right| \le i^{\tau}_{s,qs-maxi} = \sqrt{I^2_{max} - {i^{\tau}_{s,ds}}^2} \quad (25)$$

To highlight the relationship between the magnetic equation (16) and the machine load-angle δ, the vector diagram is shown in Fig. 6. According to it, the implementation of the load-angle limitation leads to the definition of the saturation limit $i^{\tau}_{s,qs-max\delta}$. This is applied regardless of the sign of the torque-producing current reference, thus leading to the following saturation law:

$$\left|i^*_{s,qs}\right| \le i^{\tau}_{s,qs-max\delta} = \tilde{\lambda}_m / \tilde{L}_s \cdot \sin\left(\delta_{max}\right) \quad (26)$$

It is noted how the load-angle limitation is performed without the use of any external controller [12], leading to a model-based regulation law that avoids demanding tuning procedures. According to [14], the load-angle limit that avoids pull-out corresponds at 90 electrical degrees, thus performing the Maximum-Torque per Voltage (MTPV) operation.

F. Voltage references computation

The predicted values of stator currents $\tilde{\bar{i}}^{\tau+1}_{s,dqs}$ and stator flux amplitude $\hat{\lambda}^{\tau+1}_s$, together with their reference values λ^*_s and $i^*_{s,qs}$, are used for the computation of the (d_s,q_s) voltage references $\bar{v}^*_{s,dqs}$. The direct and inverse rotational transformations are performed using the predicted stator flux angular position $\hat{\vartheta}^{\tau+1}_s$, as shown in Fig. 7.

The proposed predictive algorithm uses the machine inverse model for the control of the reference variables (deadbeat approach). However, two possible approaches can be adopted.

The first approach consists of inverting the discrete-time model of the machine (10). However, this operation requires the prediction of the rotor electrical position for the next sample time instant (τ+1), thus making necessary the implementation of a mechanical position observer. Nevertheless, the performance of the latter depends on accuracy in the evaluation of the mechanical parameters such as rotational inertia, friction coefficients, and load torque.

The main alternative to the first approach is represented by the application of the Euler's discretization on specific state-space equations of the machine. However, the choice of the type of equations must be properly performed to minimize the errors related to the discretization method and detuning of the machine parameters. Since one of the main goals of this work is to provide a control solution simple to be implemented, the application of the second approach is proposed.

Regardless of the considered state-space equation system, each equation has the same structure. By one side, there is the derivative of the considered variable z while, on the other one, the voltage-forcing v together with additional terms that act as additive disturbance f:

$$\frac{d}{dt}z(t) = v(t) - f(t) \tag{27}$$

Based on the operation of the discrete-time controllers, the voltage references applied at the next sample time instant (τ+1) establish the evolution of the state-variables at the next step (τ+2). Therefore, Euler's discretization of (27) leads to:

$$v^{\tau+1} = f^{\tau+1} + \frac{z^{\tau+2} - z^{\tau+1}}{T_s} \Rightarrow v^* = f^{\tau+1} + \frac{z^* - z^{\tau+1}}{T_s} \tag{28}$$

The application of (28) corresponds to invert the machine model to obtain the voltage references, thus employing a deadbeat approach. Therefore, the computation of these is performed by imposing the main variables (λ_s, $i_{s,qs}$) for the sample time instant (τ+2) with the reference ones (λ_s^*, $i_{s,qs}^*$), using specific state-space equations.

1) Predictive stator flux regulation

To obtain a simple and robust regulation of the stator flux amplitude, the d_s-axis voltage reference $v_{s,ds}^*$ is computed by applying (28) on the d_s-axis electric equation (16) as follows:

$$v_{s,ds}^* = \tilde{R}_s \cdot \tilde{i}_{s,ds}^{\tau+1} + T_s^{-1} \cdot \left(\lambda_s^* - \hat{\lambda}_s^{\tau+1}\right) \tag{29}$$

To avoid a useless reduction of the voltage margin for the q_s-axis regulation, the d_s-axis voltage reference is limited to a pre-defined voltage limit $v_{sd,max}$, however, in any case, able to ensure the stator flux amplitude regulation in all conditions.

2) Predictive torque-producing current regulation

The predictive control of the torque-producing current component can be performed using several state-space equations. However, to avoid the prediction of the load-angle for the next sample time instant (τ+1), the d_s-axis magnetic equation (16) is initially considered:

$$L_s \cdot i_{s,ds} + \lambda_m \cdot \cos(\delta) = \lambda_s \tag{30}$$

By applying the condition (9)-c) in (5), the speed deviation of the d_s-axis with respect to the physical d-axis ω_δ is defined. Therefore, by introducing its definition in (30), the following equation is obtained:

$$\omega_s \cdot L_s \cdot i_{s,ds} + \omega_r \cdot \lambda_m \cdot \cos(\delta) = \omega_\delta \cdot L_s \cdot i_{s,ds} + \omega_r \cdot \lambda_s \tag{31}$$

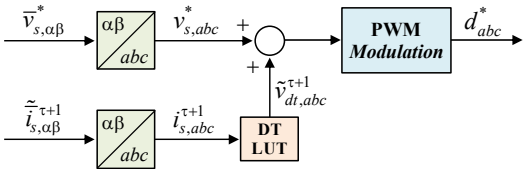

Fig. 8. Predictive compensation of dead-time voltage errors.

By replacing (31) on the q_s-axis state-space equation (17), the following result is obtained:

$$\frac{d}{dt}i_{s,qs} = -\omega_\delta \cdot i_{s,ds} - \frac{R_s}{L_s} \cdot i_{s,qs} + \frac{1}{L_s} \cdot \left(v_{s,qs} - \omega_r \cdot \lambda_s\right) \tag{32}$$

It is noted how (32) does not depend on the load-angle directly, but just on its time-variation ω_δ. However, this variable is zero in steady-state conditions, making this form of the q_s-axis state-space equation robust and straightforward. Therefore, by applying (28) on (32), the q_s-axis voltage reference $v_{s,qs}^*$ is computed as follows:

$$v_{s,qs}^* = \tilde{R}_s \cdot \tilde{i}_{s,qs}^{\tau+1} + \tilde{\omega}_\delta^{\tau+1} \cdot \tilde{L}_s \cdot \tilde{i}_{s,ds}^{\tau+1} + \omega_r^{\tau+1} \cdot \hat{\lambda}_s^{\tau+1} + \frac{\tilde{L}_s}{T_s} \cdot \left(i_{s,qs}^* - \tilde{i}_{s,qs}^{\tau+1}\right) \tag{33}$$

G. PWM modulation

Once the components of the voltage reference vector in the rotating (d_s,q_s) frame are obtained, the inverse reference transformations are implemented (rotational plus Clarke), leading to the computation of the voltage reference vector in phase coordinates $v_{s,abc}^*$. Finally, the computation of the duty-cycles d_{abc}^* is performed, as shown in Fig. 8. Therefore, based on the deadbeat schemes, a PWM modulator is employed, without the use of any cost function and using well-known PWM techniques [18]. In this work, the 'Min-Max' modulation has been implemented.

Moreover, by using the predicted values of the stator currents, the Dead-Time (DT) errors of the power converter for the next sample time instant (τ+1) are estimated [16]. In this way, a feed-forward compensation of the inverter DT voltage errors is performed, as shown in Fig. 8. This action leads to significant improvements in the current waveforms, especially at low speed and for the no-load conditions.

IV. Experimental validation

The machine used for the experimental validation is a low-power (600 W) fractional slot SPM machine having 42 poles and outer rotor for direct drive applications (Fig. 9). The machine maximum speed is 1200 rpm while the maximum fundamental frequency is 420 Hz. The main features of the machine are reported in the Appendix.

A. Test rig

The machine has been mounted on a test rig for validation. The rotor shaft has been coupled to a driving machine acting as a prime mover, as shown in Fig. 9. The power converter consists of a three-phase inverter fed by a conventional bridge rectifier with a single-phase ac supply (230 Vrms @ 50 Hz), leading to an average DC link voltage of about 310V.

The switching frequency and the sampling frequency have been set at 16 kHz (inverter dead-time 1 μs), corresponding to the target values used for this kind of application (to reduce the switching noise). The digital controller is the dSPACE® DS1103 fast prototyping board while the control algorithm has been totally developed in the C-code environment.

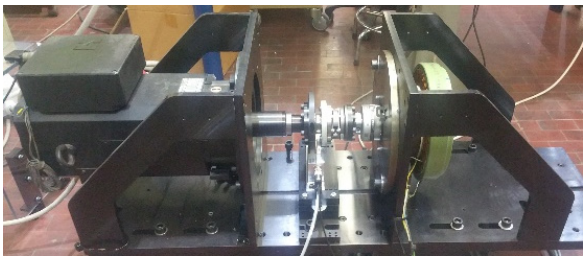

Fig. 9. View of the machine under test (right) and the driving machine (left).

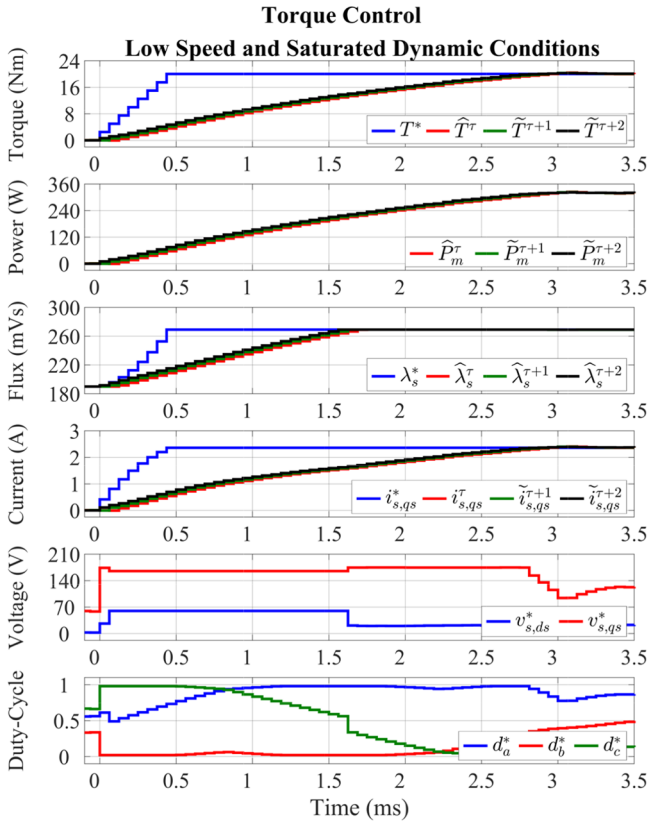

Fig. 10. High slew-rate torque transient from no-load up to 100% rated torque (20 Nm) at 150 rpm. From top to bottom: reference, observed and predicted torque (Nm); estimated and predicted mechanical power (W); reference, observed and predicted stator flux amplitude (mVs); reference, measured and predicted q_s-axis current (A); (d_s,q_s) voltage references (V); inverter duty-cycles.

B. *Experimental results*

The experimental results are related to the drive operation in both torque control mode and speed control mode. To demonstrate the robustness of the discretization process, a double-step prediction action has been performed. In this way, the predictions of the stator flux vector and the stator current vector at next (τ+2) sampling instant have been obtained (not used in the control scheme, only for visualization purposes).

1) Torque control in motoring mode at low-speed

The torque transient from zero to the positive rated value (20 Nm) is shown, at a constant speed of 150 rpm (electric frequency 50 Hz) imposed by the driving machine (Fig. 10). To highlight the MTPA operation, the torque reference has been set to a ramp with a high slew-rate (40 Nm/ms). Due to the consequent high slew-rate of both references of stator flux amplitude and torque-producing current, the (d_s,q_s) reference voltages have reached their respective saturation limits (where $v_{sd,max}$ = 60 V) as confirmed by the saturation of the inverter duty-cycles, as shown in Fig. 10.

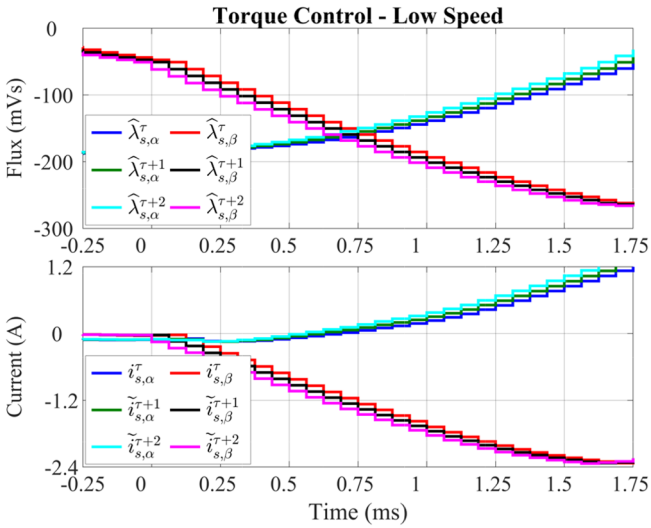

Fig. 11. High slew-rate torque transient from no-load up to 100% rated torque (20 Nm) at 150 rpm. From top to bottom: observed and predicted stator flux components in the stationary (α,β) frame (mVs); observed and predicted stator current components in the stationary (α,β) frame (A).

For this reason, the profile of the torque reference is not followed, corresponding to the operation of the drive under saturated dynamic conditions. However, the proposed control solution can impose the reference values of stator flux amplitude and torque-producing current without any overshoot, with the best dynamic response. Consequently, also the dynamic torque response has the same behavior.

It is noted how below the base speed (300 rpm), the MTPA operation has been perfectly fulfilled. Finally, the predicted values of stator flux, stator currents and, electromagnetic torque are estimated properly for both (τ+1) and (τ+2) sampling instants, as shown in Figs. 10-11.

2) Torque control with the reversal operation from generation mode to motoring mode at low speed

The torque step response from the negative rated value to the positive one (from -20 Nm to 20 Nm), at a constant speed of 100 rpm (electric frequency 35 Hz), is shown in Figs. 12-13. It is noted how the torque reversal is performed in the shortest possible rise time, without any overshoot and, with zero steady-state error (Fig. 13), thus demonstrating the deadbeat behavior of the proposed control solution.

Since only the sign of the torque reference is reversed, the MTPA value of stator flux amplitude reference does not change. Therefore, only the regulation of the torque-producing current is performed, demonstrating the high level of decoupling between the (d_s,q_s) control axes. As for the previous test, the predicted values of stator flux, stator currents and, electromagnetic torque are estimated properly for both (τ+1) and (τ+2) sampling instants, as shown in Fig. 12.

Due to the high slew-rate of the torque (4000 Nm/s), the driving machine has not been able to keep the speed at the constant value of 100 rpm (deviation of about 50 rpm), as shown in Fig. 12. Therefore, although the torque has been correctly reversed, the mechanical power has not followed the same profile (from -210 W up to 450 W). For this reason, the absolute values of load-angle before and after the torque reversal result different (Fig. 12). However, this is further proof of the robustness of the proposed control solution, able to operate in a scenario in which electromagnetic and mechanical variables are both in transient conditions.

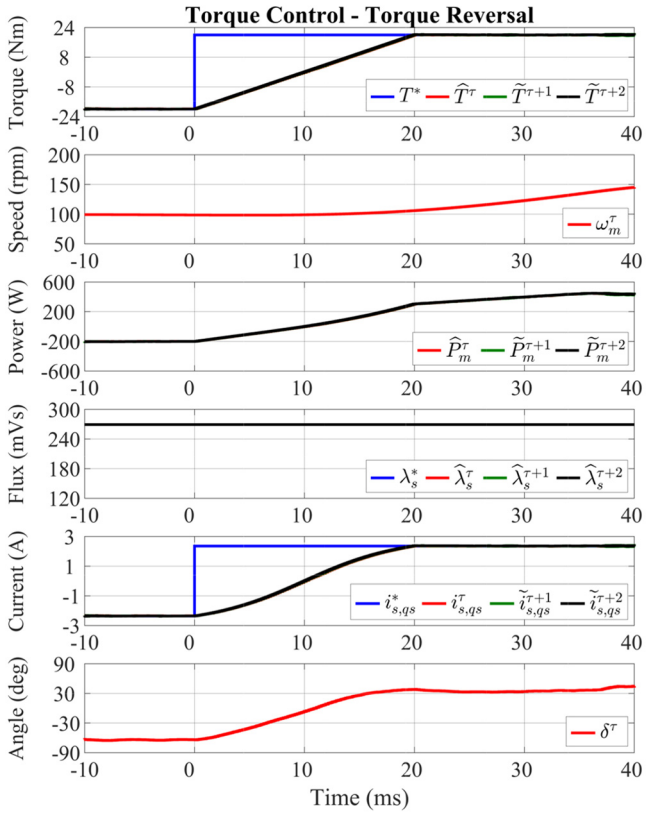

Fig. 12. Step response from 100% rated torque in generation to 100% rated torque in motoring at 100 rpm. From top to bottom: reference, observed and predicted torque (Nm); measured mechanical speed (rpm); estimated and predicted mechanical power (W); reference, observed and predicted stator flux amplitude (mVs); reference, measured and predicted q_s-axis current (A); observed load-angle (deg).

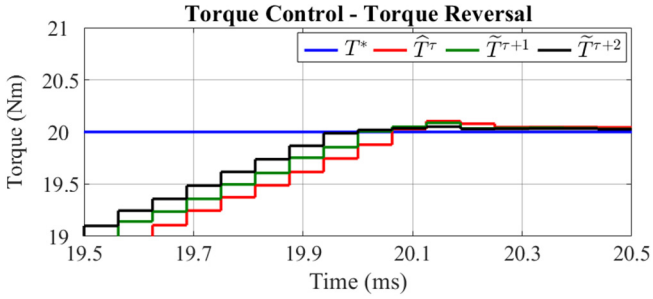

Fig. 13. Step response from 100% rated torque in generation to 100% rated torque in motoring at 100 rpm. Magnification of Fig. 12: reference, observed and predicted torque (Nm).

3) Torque control in flux-weakening operation

The validation of the drive under both voltage and current constraints has been obtained through the maximum-torque per speed profile, as shown in Fig. 14. During the test, the machine has been torque-controlled with a reference torque equal to the rated value (20 Nm).

The mechanical speed has been set to an initial value of 100 rpm (electric frequency 35 Hz). In this condition, the drive was operated without any limitation in terms of voltage and current. Through the driving machine, the mechanical speed has been increased to the maximum value of 1200 rpm (electric frequency 420 Hz) with a slew rate of 400 rpm/s. Above the base speed (≅240 rpm), the torque has been reduced according to the current and voltage limitations, obtaining a constant mechanical power of 600 W.

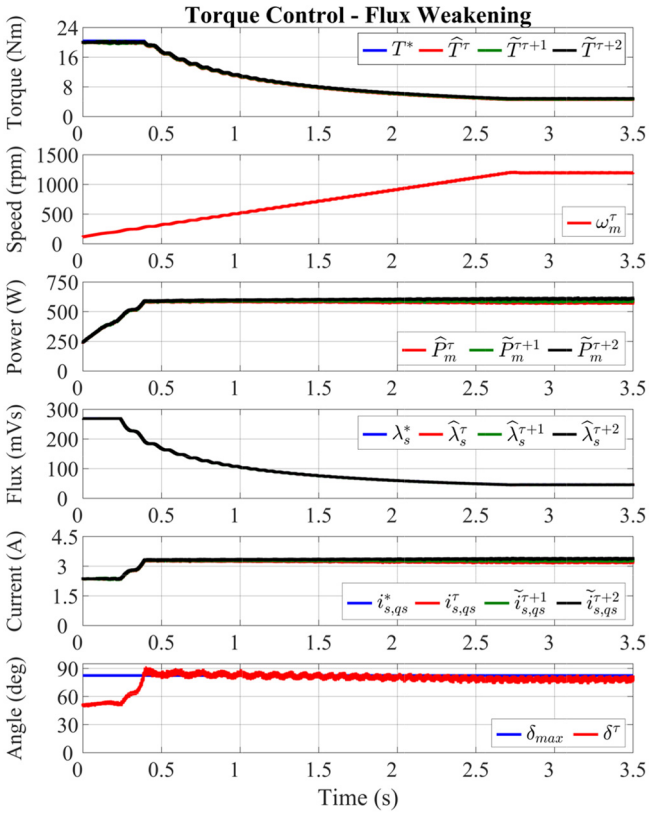

Fig. 14. Torque control in flux weakening during the speed transient from 100 rpm to 1200 rpm. From top to bottom: reference, observed and predicted torque (Nm); measured mechanical speed (rpm); estimated and predicted mechanical power (W); reference, observed and predicted stator flux amplitude (mVs); reference, measured and predicted q_s-axis current (A); maximum and observed load-angle (deg).

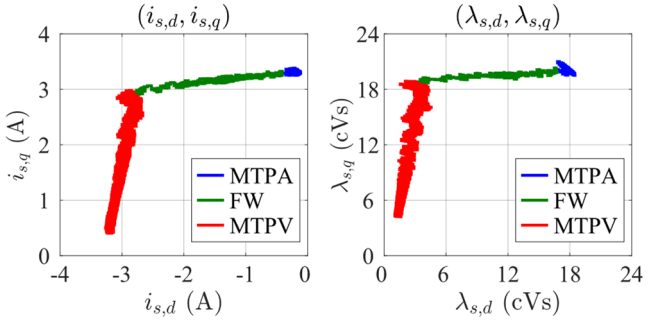

Fig. 15. Torque control in flux weakening during the speed transient from 100 rpm to 1200 rpm. From left to right: stator current vector position in the physical (d,q) frame; stator flux vector position in the physical (d,q) frame.

The predicted values of stator flux, stator currents and, electromagnetic torque are estimated properly for both (τ+1) and (τ+2) sampling instants in the complete speed range (Fig. 14). During the speed transient, the drive can guarantee the maximum torque production without any stability issue (constant power range of 600 W kept without any problem). It is noted the deep flux-weakening operation (flux weakening ratio 1:5).

The MTPV limitation becomes active when the maximum load-angle is reached, at a speed of about 300 rpm. For safety, the maximum load-angle has been set at δ_{max} = 80 electrical degrees to avoid the machine pull-out. As can be seen in Fig. 14, at MTPV operation, the load-angle is properly limited.

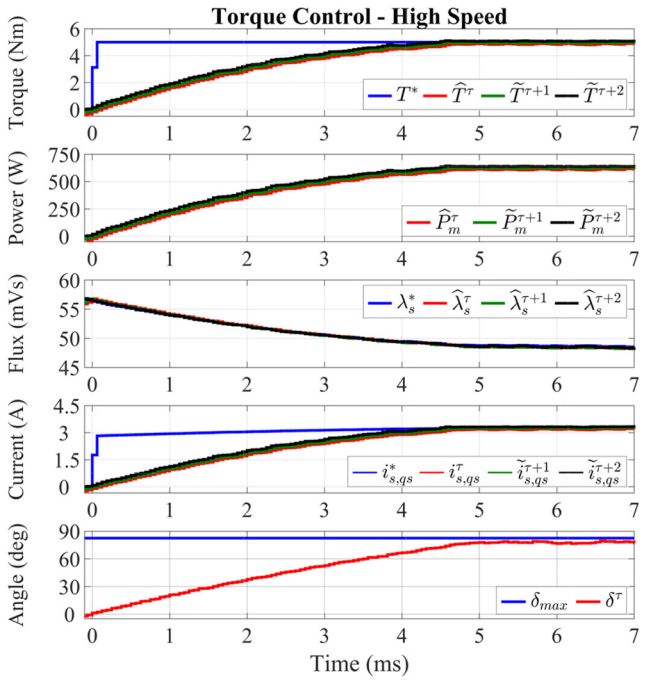

Fig. 16. High slew-rate torque transient from no-load up to the maximum allowable torque (≅ 5 Nm) at 1200 rpm. From top to bottom: reference, observed and predicted torque (Nm); estimated and predicted mechanical power (W); reference, observed and predicted stator flux amplitude (mVs); reference, measured and predicted q_s-axis current (A); maximum and observed load-angle (deg).

Furthermore, there is the full correspondence between the variables controlled by the DFVC scheme (λ_s,$i_{s,qs}$) with those referred in the physical (d,q) frame (Fig. 15). During the MTPA operation, corresponding to the injection of current on the q-axis, the d-axis current is practically zero. In FW operation, based on the stator flux amplitude reference, negative values of the d-axis current are imposed. In this way, the d-axis flux component is reduced, thus compensating the PM contribution. Finally, in MTPV operation, both (d,q) stator current and flux components are reduced (Fig. 15), as foreseen by the FOC theory.

4) Torque control at high-speed

The torque transient with a high slew rate (40 Nm/ms) from zero to the maximum allowable torque (≅ 5 Nm), at the maximum speed of 1200 rpm (electrical frequency 420 Hz), is shown in Fig. 16.

The predicted values of stator flux, stator currents and, electromagnetic torque are estimated properly for both (τ+1) and (τ+2) sampling instants, demonstrating the validity of the discretization method also at the maximum fundamental frequency, as shown in Figs. 16-17.

The operation at the maximum torque corresponds with the MTPV operation of the drive. Indeed, the torque-producing current component is limited to the value defined by (26). The load-angle has been limited without any issue, despite its strong variation from zero (no-load condition) to the maximum allowable value (80 electrical degrees).

Finally, it is noted how the reference values of stator flux amplitude and torque-producing current have been imposed without any overshoot, demonstrating a high level of decoupling among the (ds,qs) control axes, as foreseen by the DFVC approach.

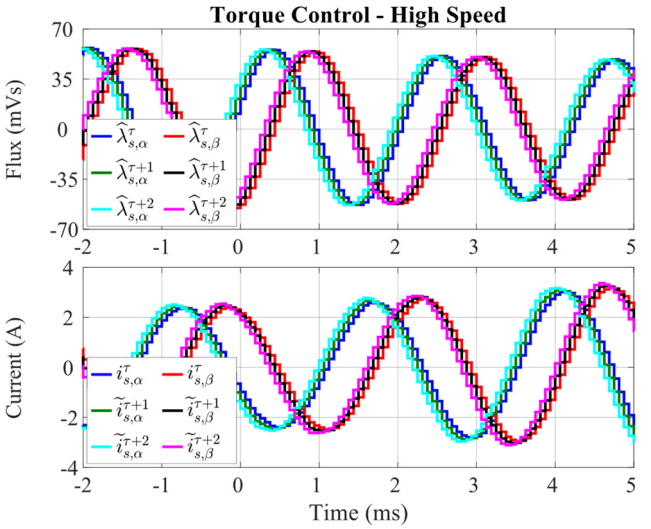

Fig. 17. High slew-rate torque transient from no-load up to the maximum allowable torque (≅ 5 Nm) at 1200 rpm. From top to bottom: observed and predicted stator flux components in the stationary (α,β) frame (mVs); observed and predicted stator current components in the stationary (α,β) frame (A).

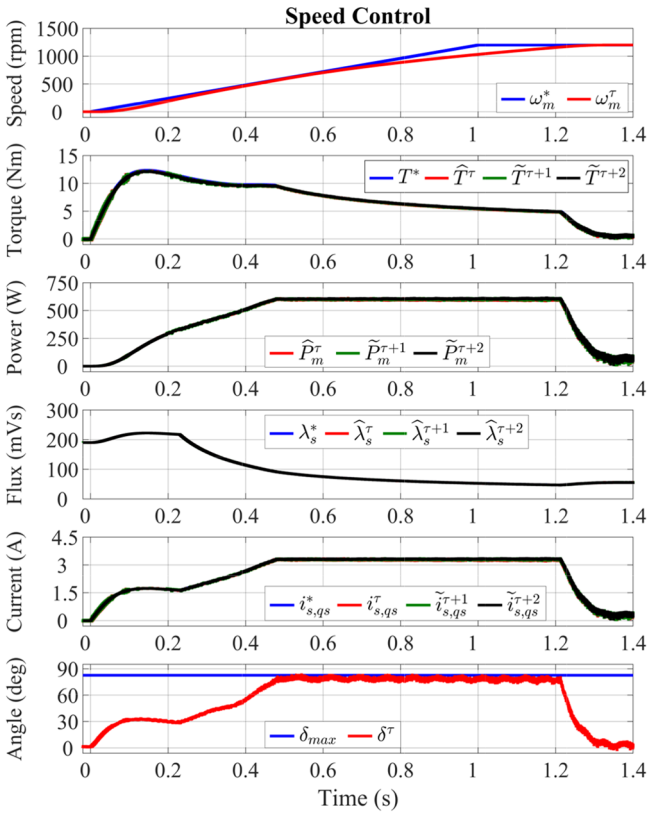

Fig. 18. Speed control with inertial load from 0 to 1200 rpm. From top to bottom: reference and measured mechanical speed (rpm); reference, observed and predicted torque (Nm); estimated and predicted mechanical power (W); reference, observed and predicted stator flux amplitude (mVs); reference, measured and predicted q_s-axis current (A); maximum and observed load-angle (deg).

5) Closed-loop speed control

The closed-loop speed control has been tested with the driving machine acting as an inertial load. The speed control has been implemented with a PI controller whose output is the reference torque provided to the DB-DFVC scheme. The obtained results for a speed transient from 0 up to 1200 rpm are shown in Fig. 18. To avoid dangerous mechanical stresses for the test rig, the acceleration has been limited at 1200 rpm/s.

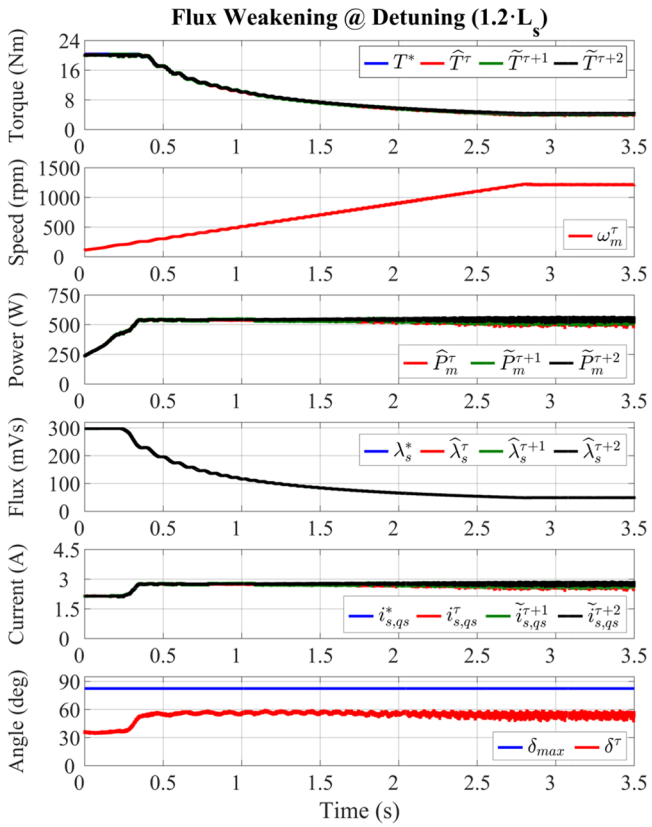

Fig. 19. Torque control in flux weakening during the speed transient from 100 rpm to 1200 rpm, using $\hat{L}_s = 1.2L_s$. From top to bottom: reference, observed and predicted torque (Nm); measured mechanical speed (rpm); estimated and predicted mechanical power (W); reference, observed and predicted stator flux amplitude (mVs); reference, measured and predicted q_s-axis current (A); maximum and observed load-angle (deg).

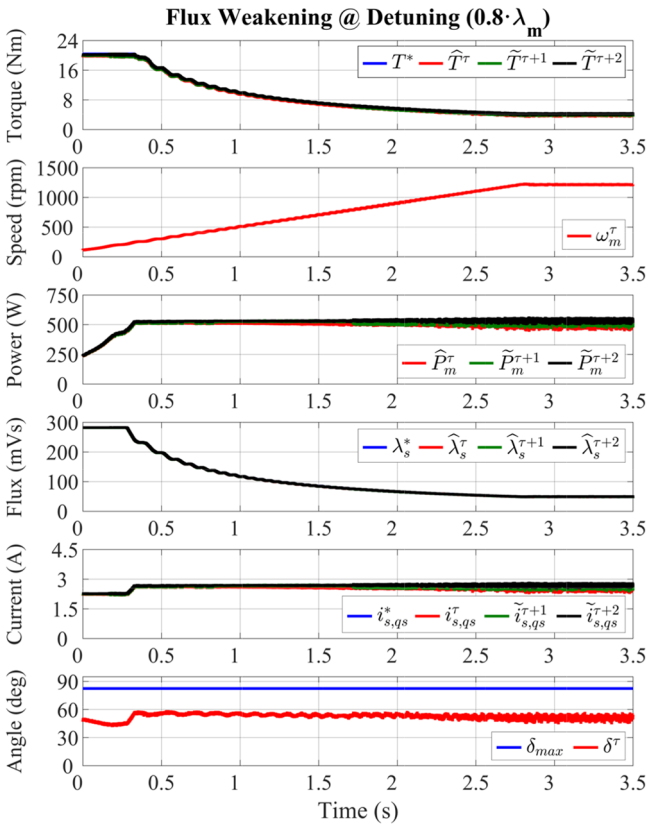

Fig. 20. Torque control in flux weakening during the speed transient from 100 rpm to 1200 rpm, using $\hat{\lambda}_m = 0.8\lambda_m$. From top to bottom: reference, observed and predicted torque (Nm); measured mechanical speed (rpm); estimated and predicted mechanical power (W); reference, observed and predicted stator flux amplitude (mVs); reference, measured and predicted q_s-axis current (A); maximum and observed load-angle (deg).

Due to the limited slew rate of the speed reference, the initial torque reference results quite lower than the rated value (maximum value near to 12 Nm). For this reason, the voltage and current limitations become active at different operating speeds. In detail, the FW starts at speed near to 240 rpm, corresponding to the operation of the drive under the condition of voltage limitation only. Conversely, the current limitation, corresponding to the MTPV operation, becomes active at a speed of about 550 rpm.

It is noted how the considerations made in torque control mode are still valid. Therefore, the proposed solution is compatible with drive schemes where the torque reference is provided by an outer controller.

6) Performance in detuning conditions

According to the literature [9], [19], the performance of a deadbeat control scheme depends on the detuning of the machine parameters and discretization errors [20]. In this work, since an accurate discrete-time model of the machine is used (10)-(11), only the performance of the proposed solution in the case of the detuning of the machine parameters is considered.

Based on (21), the performance of the MPE is dependent on the accuracy at evaluating the stator inductance L_s and PM flux linkage λ_m. For this reason, two realistic scenarios have been emulated, testing the detuning effects of these two parameters. However, it is highlighted how these tests represent only a preliminary analysis of the robustness of the proposed solution, the latter being the future development of this work.

a) Detuning on the stator inductance

The first scenario concerns the overestimation of the stator inductance, thus neglecting possible effects related to the magnetic saturation. More specifically, test "*3) Torque control in flux-weakening operation*" has been again performed, using $\hat{L}_s = 1.2L_s$. The obtained results are shown in Fig. 19. It is noted how the detuning of the stator inductance affects the performance of the control scheme in MTPA and MTPV operations. Regarding the MTPA operation, since a model-based regulation law (22) is used, the overestimation of the stator inductance leads to a slight overestimation of the optimal stator flux amplitude reference.

For the MTPV operation, the considered inductance detuning leads to the under-estimation of the torque-producing current limit (26). Therefore, a loss in torque/power production is reported. Indeed, compared to the case without the detuning of the machine parameters (Fig. 14), a loss of the mechanical power near to 17% is noted (from 600 W to 500 W). This is also confirmed by the load-angle value that results lower than the upper limit (from 80 to 55 electrical degrees), as shown in Fig. 19. However, it must be underlined here that a FOC with inner current control loops will roughly get the same effects, as the control scheme will limit the negative d-axis current to the characteristic current $(-\hat{\lambda}_m/\hat{L}_s)$ that results underestimated for the considered detuning condition.

A possible solution robust to parameter detuning to this issue is represented by the adoption of a load angle compensation mechanism, like that used in [12] for DFVC, thus avoiding the loss in the torque/power production.

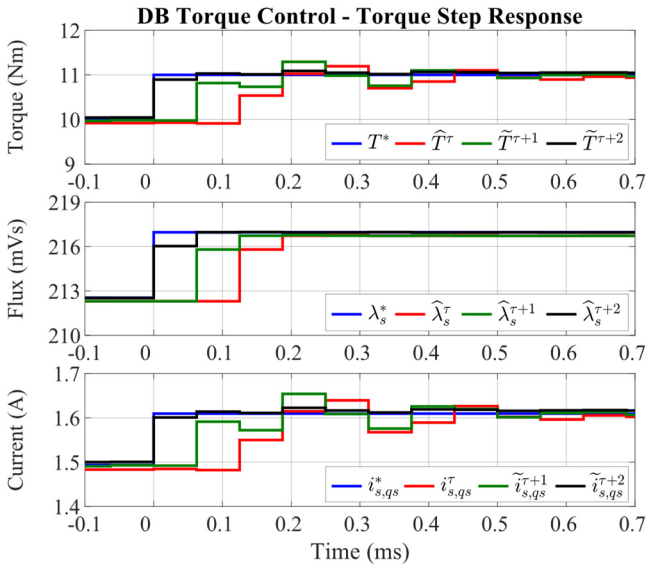

Fig. 21. Step response from 10 Nm to 11 Nm at 100 rpm using DB controllers. From top to bottom: reference, observed and predicted torque (Nm); reference, observed and predicted stator flux amplitude (mVs); reference, measured and predicted q_s-axis current (A).

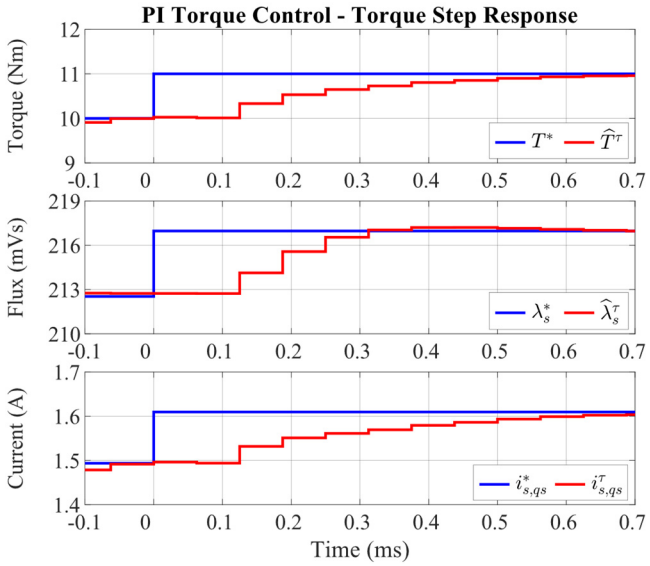

Fig. 22. Step response from 10 Nm to 11 Nm at 100 rpm using PI controllers. From top to bottom: reference and observed torque (Nm); reference and observed stator flux amplitude (mVs); reference and measured q_s-axis current (A).

As shown in Fig. 19, no instability has been noted, although the noise level increases due to the prediction errors made by the MPE.

b) Detuning on the PM flux linkage

The second scenario consists of an underestimation of the PM flux linkage. Therefore, the torque control has been tested using $\hat{\lambda}_m = 0.8\lambda_m$. It is noted how the detuning on this parameter leads to similar effects to those of the first scenario, as shown in Fig. 20. For the MTPA operation, according to the model-based regulation law (22), the underestimation of the PM flux linkage leads to an underestimation of the optimal stator flux amplitude reference.

For the MTPV operation, no instability has been noted, although the noise level increases due to the prediction errors made by the MPE, as shown in Fig. 20. The effects on the limitation of the load angle are similar with the previous case.

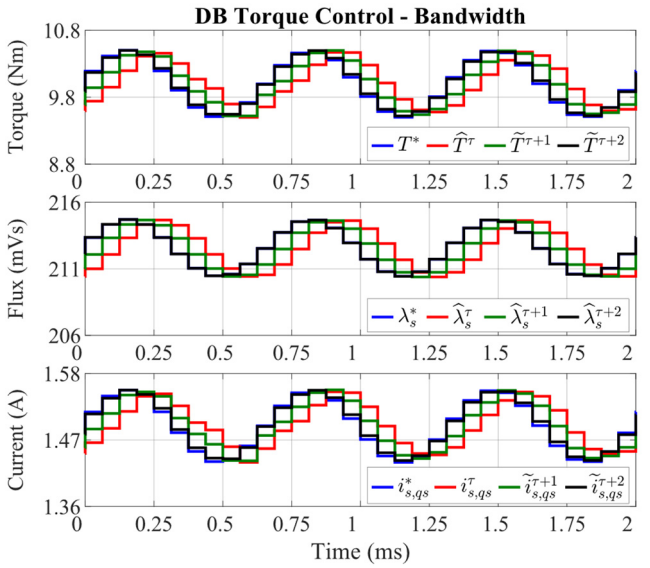

Fig. 23. Bandwidth response at 100 rpm using DB controllers. From top to bottom: reference, observed and predicted torque (Nm); reference, observed and predicted stator flux amplitude (mVs); reference, measured and predicted q_s-axis current (A).

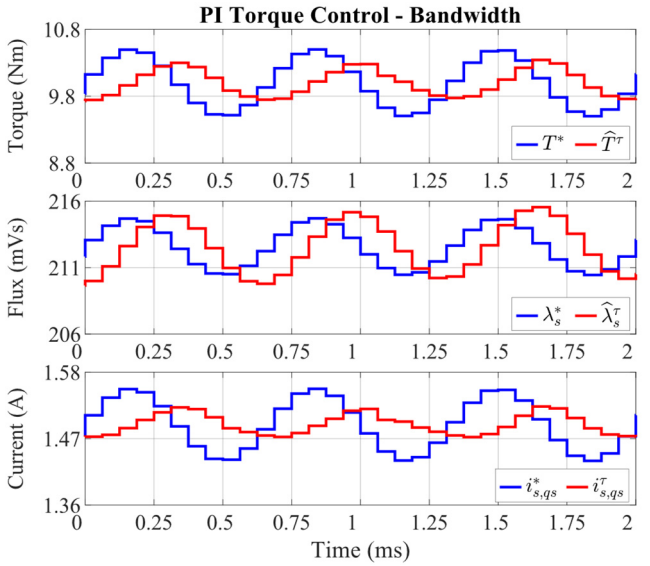

Fig. 24. Bandwidth response at 100 rpm using PI controllers. From top to bottom: reference and observed torque (Nm); reference and observed stator flux amplitude (mVs); reference and measured q_s-axis current (A).

The same effects will be obtained for the FOC with inner control loops, as the control scheme will limit the negative d-axis current to the characteristic current $(-\hat{\lambda}_m/\hat{L}_s)$ that results underestimated. The solution to counteract the detuning on magnets flux is to roughly adapt the magnets flux with the temperature using schemes that are beyond the scope of the paper as it does not depend on the adopted control scheme.

7) Comparison between DB-DFVC and PI-DFVC

To demonstrate that the deadbeat controllers (DB-DFVC) lead to better dynamic performance to a DFVC scheme that uses PI regulators (PI-DFVC), several comparisons between these two control solutions have been performed.

The bandwidth of the PI controllers has been set at 1 kHz. More details about the PI-DFVC scheme can be found in [12]. However, to perform a fair comparison, the PI-DFVC solution has been improved using calibrated feed-forward voltage

terms, thus compensating the time-derivatives of the control variables (stator flux amplitude and torque-producing current component). In this way, the best dynamic performance of the PI-DFVC solution has been obtained.

a) Step response – small torque reference variation

The first comparison has been performed by testing the step response of the two control solutions in the case of a small reference torque variation is applied. In both cases, the drive has been tested in torque control mode, at a constant speed of 100 rpm imposed by the driving machine. The reference torque has been initially set at 10 Nm. From a random instant of time onwards, the reference torque has been suddenly set at 11 Nm. The responses of both DB-DFVC and PI-DFVC solutions are reported in Figs. 21-22.

Thanks to the one-step-ahead prediction of the control variables, the proposed DB-DFVC can satisfy the torque target in one sampling period (Fig. 21), corresponding to the minimum response time of a digital electric drive. The small oscillations in the current/torque response are produced by a non-ideal current acquisition, as happens in industrial drives. However, this factor does not affect the dynamic performance of the DB-DFVC scheme, as shown in Fig. 21.

Based on Fig. 22, it is noted how the PI-DFVC solution has required much more time to satisfy the torque target (eleven sampling periods), thus demonstrating the significant improvement obtained with the implementation of the DB-DFVC scheme. Besides, since the prediction of the control variables is not performed, the results of the PI-DFVC scheme contains only observed and measured values (Fig. 22).

b) Verification of torque control bandwidth

The second comparison consisted of testing the bandwidth of both torque control solutions. The drive has been tested in torque control mode, at a constant speed of 100 rpm imposed by the driving machine. A constant reference torque of 10 Nm has been set. In addition, a sinusoidal reference torque having an amplitude of 0.5 Nm and a frequency of 1.5 kHz has been added. The responses obtained by DB-DFVC and PI-DFVC are reported in Figs. 23-24.

Compared to the conventional PI-DFVC scheme (Fig. 24), the DB-DFVC has been able to follow the reference torque without any problem, as shown in Fig. 23. It is noted the deadbeat behavior of the DB-DFVC scheme in which reference torque, predicted torque (τ+1), and observed torque (τ) are shifted to each other in time by one sampling period. Finally, the demonstration of the equation (28) is also provided. Indeed, the predicted torque for the sampling time (τ+2) corresponds to the reference value, as shown in Fig. 21, and Fig. 23.

V. Conclusion

The paper proposes a predictive torque control for surface permanent magnet motor drives. The predictive algorithm uses a deadbeat approach and it is implemented on the structure of the direct flux vector control scheme, allowing the simultaneous control of the stator flux amplitude and torque-producing current.

The performance of the proposed control solution has been validated with a fractional slot surface permanent magnet machine designed for deep flux weakening. The proposed solution is suitable for applications that require a wide constant power range such as traction drives with in-wheel motors with concentrated windings.

The experimental results demonstrate the torque control performance in the full speed range of the drive, with current and voltage limitations. The deadbeat torque control is able to work properly with saturated voltage commands and avoids motor pull-out at high speed using a proper load-angle limitation corresponding to the maximum torque per volt operation. The control stability of the proposed solution in the case of heavy detuning of the machine parameters is also demonstrated. Besides, a comparison between the proposed scheme and the one using conventional proportional-integral controllers is provided, thus demonstrating the obtained dynamic improvement in the torque response.

Appendix

The machine parameters are reported in Table I.

TABLE I. SPM Machine Parameters

Pole pairs p	21
Stator resistance R_s	7.1 Ω
Stator inductance L_s	57 mH
Permanent magnet flux linkage λ_m	0.19 Vs
Rated torque	20 Nm
Maximum speed	1200 rpm
Rated current (rms)	2.5 A
Overall rotational inertia	0.021 kg·m^2

References

[1] P. Cortes, M. P. Kazmierkowski, R. M. Kennel, D. E. Quevedo, and J. Rodriguez, 'Predictive Control in Power Electronics and Drives', *IEEE Trans. Ind. Electron.*, vol. 55, no. 12, pp. 4312–4324, Dec. 2008.

[2] M. Preindl and S. Bolognani, 'Model Predictive Direct Torque Control With Finite Control Set for PMSM Drive Systems, Part 1: Maximum Torque Per Ampere Operation', *IEEE Trans. Ind. Inform.*, vol. 9, no. 4, pp. 1912–1921, Nov. 2013.

[3] M. Preindl and S. Bolognani, 'Model Predictive Direct Torque Control With Finite Control Set for PMSM Drive Systems, Part 2: Field Weakening Operation', *IEEE Trans. Ind. Inform.*, vol. 9, no. 2, pp. 648–657, May 2013.

[4] A. A. Ahmed, B. K. Koh, and Y. I. Lee, 'A Comparison of Finite Control Set and Continuous Control Set Model Predictive Control Schemes for Speed Control of Induction Motors', *IEEE Trans. Ind. Inform.*, vol. 14, no. 4, pp. 1334–1346, Apr. 2018.

[5] J. Scoltock, T. Geyer, and U. K. Madawala, 'A Comparison of Model Predictive Control Schemes for MV Induction Motor Drives', *IEEE Trans. Ind. Inform.*, vol. 9, no. 2, pp. 909–919, May 2013.

[6] C. Choi, J. Seok, and R. D. Lorenz, 'Wide-Speed Direct Torque and Flux Control for Interior PM Synchronous Motors Operating at Voltage and Current Limits', *IEEE Trans. Ind. Appl.*, vol. 49, no. 1, pp. 109–117, Jan. 2013.

[7] J. S. Lee, C. Choi, J. Seok, and R. D. Lorenz, 'Deadbeat-Direct Torque and Flux Control of Interior Permanent Magnet Synchronous Machines With Discrete Time Stator Current and Stator Flux Linkage Observer', *IEEE Trans. Ind. Appl.*, vol. 47, no. 4, pp. 1749–1758, Jul. 2011.

[8] J. S. Lee and R. D. Lorenz, 'Deadbeat Direct Torque and Flux Control of IPMSM Drives Using a Minimum Time Ramp Trajectory Method at Voltage and Current Limits', *IEEE Trans. Ind. Appl.*, vol. 50, no. 6, pp. 3795–3804, Nov. 2014.

[9] J. S. Lee and R. D. Lorenz, 'Robustness Analysis of Deadbeat-Direct Torque and Flux Control for IPMSM Drives', *IEEE Trans. Ind. Electron.*, vol. 63, no. 5, pp. 2775–2784, May 2016.

[10] Y. Wang *et al.*, 'Deadbeat Model-Predictive Torque Control With Discrete Space-Vector Modulation for PMSM Drives', *IEEE Trans. Ind. Electron.*, vol. 64, no. 5, pp. 3537–3547, May 2017.

[11] G. Scarcella, G. Scelba, M. Pulvirenti, and R. D. Lorenz, 'Fault-Tolerant Capability of Deadbeat-Direct Torque and Flux Control for Three-Phase PMSM Drives', *IEEE Trans. Ind. Appl.*, vol. 53, no. 6, pp. 5496–5508, Nov. 2017.

[12] G. Pellegrino, R. I. Bojoi, and P. Guglielmi, 'Unified Direct-Flux Vector Control for AC Motor Drives', *IEEE Trans. Ind. Appl.*, vol. 47, no. 5, pp. 2093–2102, Sep. 2011.

[13] S. Rubino, R. Bojoi, E. Armando, and A. Tenconi, 'Model Predictive Direct Flux Vector Control of Surface Permanent Magnet Motor Drives', in *2018 IEEE Energy Conversion Congress and Exposition (ECCE)*, 2018, pp. 5458–5465.

[14] P. Krause, O. Wasynczuk, S. D. Sudhoff, and S. Pekarek, *Analysis of Electric Machinery and Drive Systems*. John Wiley & Sons, 2013.

[15] R. Isermann, *Digital Control Systems: Volume 1: Fundamentals, Deterministic Control*. Springer Science & Business Media, 2013.

[16] I. R. Bojoi, E. Armando, G. Pellegrino, and S. G. Rosu, 'Self-commissioning of inverter nonlinear effects in AC drives', in *2012 IEEE International Energy Conference and Exhibition (ENERGYCON)*, 2012, pp. 213–218.

[17] E. Armando, R. I. Bojoi, P. Guglielmi, G. Pellegrino, and M. Pastorelli, 'Experimental Identification of the Magnetic Model of Synchronous Machines', *IEEE Trans. Ind. Appl.*, vol. 49, no. 5, pp. 2116–2125, Sep. 2013.

[18] D. G. Holmes and T. A. Lipo, *Pulse Width Modulation for Power Converters: Principles and Practice*. John Wiley & Sons, 2003.

[19] W. Xu and R. D. Lorenz, 'Reduced Parameter Sensitivity Stator Flux Linkage Observer in Deadbeat-Direct Torque and Flux Control for IPMSMs', *IEEE Trans. Ind. Appl.*, vol. 50, no. 4, pp. 2626–2636, Jul. 2014.

[20] W. Xu and R. D. Lorenz, 'Low-Sampling-Frequency Stator Flux Linkage Observer for Interior Permanent-Magnet Synchronous Machines', *IEEE Trans. Ind. Appl.*, vol. 51, no. 5, pp. 3932–3942, Sep. 2015.